Chaos, Solitons & Fractals 43 (2010) 57–67

Contents lists available at ScienceDirect

Chaos, Solitons & Fractals

Nonlinear Science, and Nonequilibrium and Complex Phenomena

journal homepage: www.elsevier.com/locate/chaos

Multifractal analysis of three-dimensional histogram from color images

Julien Chauveau, David Rousseau, Paul Richard, François Chapeau-Blondeau *

Laboratoire d'Ingénierie des Systèmes Automatisés (LISA), Université d'Angers, 62 avenue Notre Dame du Lac, 49000 Angers, France

ARTICLE INFO

Article history:
Received 1 June 2010
Accepted 30 August 2010

ABSTRACT

Natural images, especially color or multicomponent images, are complex information-carrying signals. To contribute to the characterization of this complexity, we investigate the possibility of multiscale organization in the colorimetric structure of natural images. This is realized by means of a multifractal analysis applied to the three-dimensional histogram from natural color images. The observed behaviors are confronted to those of reference models with known multifractal properties. We use for this purpose synthetic random images with trivial monofractal behavior, and multidimensional multiplicative cascades known for their actual multifractal behavior. The behaviors observed on natural images exhibit similarities with those of the multifractal multiplicative cascades and display the signature of elaborate multiscale organizations stemming from the histograms of natural color images. This type of characterization of colorimetric properties can be helpful to various tasks of digital image processing, as for instance modeling, classification, indexing.

1. Introduction

Natural images, especially color or multicomponent images, constitute information-carrying structures that can exhibit complex organizations. A window on this complexity is provided by their histogram, which represent multidimensional data structures that can themselves display complex organizations [1,2]. This can, for instance, be manifested by concentrations of pixels in certain regions of the histogram, with other regions void of pixels, or clusters of pixels of various sizes and densities non uniformly scattered. An illustration of such complex organization is depicted, for a natural RGB color image from Fig. 1, by the three-dimensional histogram presented in Fig. 2. The characterization of such complex organizations in multidimensional histograms is useful to image modeling and efficient exploitation of their histograms, for instance to identify relevant structures or clusters for segmentation, classification, indexing, or other purposes, or to envisage reduction of dimensionality. Many image processing tasks can benefit from approaches that start to operate on an approximate raw description at coarse scales or resolutions, while controlling the progressive refinements of the description towards finer resolutions as needed. Such approaches could benefit from characterizations across scales providing a point of view on how relevant features in images distribute, and possibly relate to each other, at various scales or resolutions. To contribute to the characterization of such complex organizations, we realize here a multifractal analysis of three-dimensional histograms from natural color images, which will reveal elaborate structures across scales.

Fractal and multifractal concepts so far have been applied essentially to the spatial organization of images [3–9]. Fractal or self-similarity properties have been reported in the spatial organization of natural images [10,4,11], and related to the many features and details usually present across many spatial scales, in a self-similar way, in natural scenes. Multifractal concepts have been employed to analyze and synthesize complex textures or gray-level statistics extending spatially over natural images [12–19]. These fractal and multifractal approaches of the spatial properties are helpful to construct more realistic models for natural images, and carry relevance for image coding and processing [20–22] and vision systems [23,24].

* Corresponding author.
E-mail address: chapeau@univ-angers.fr (F. Chapeau-Blondeau).

0960-0779/$ - see front matter © 2010 Elsevier Ltd. All rights reserved.
doi:10.1016/j.chaos.2010.08.003

Fig. 1. Two RGB color images with $N_{tot} = 512 \times 512$ pixels and $Q = 256$ levels.

In the present paper, we will examine another, complementary, aspect of the fractal and multifractal properties of natural images. Beyond the spatial organization of natural images, we address here their colorimetric organization. Some evidence has recently been reported that fractal or self-similar structurations could also exist in the colorimetric domain for natural images [25,26]. The pixels of natural color images would tend to display, over the colorimetric space, specific organizations with self-similar fractal arrangements. This has been shown by means of the evaluations of the correlation dimension in [25], and of the capacity dimension in [26], of the distribution of pixels in the colorimetric space, as represented by the three-dimensional color histogram of the images. We complement these colorimetric characterizations by investigating here the full spectrum of fractal dimensions [27,28], via a multifractal analysis, which is performed for the first time from the three-dimensional color histograms as done here.

2. Multifractal analysis

We consider color images where each of the N_{tot} pixels is represented by a triplet of components (R,G,B), each of these components assuming an integer value in $[0, Q-1]$ (for example $Q = 2^8 = 256$). The three-dimensional space of color coordinates (R,G,B) therefore possesses Q^3 colorimetric cells or distinct colors. The pixels distributed among these colorimetric cells form the three-dimensional histogram of the image. For common natural color images as we shall analyze (see Fig. 1), Fig. 2 shows a three-dimensional histogram under two different angles of view, for a visual appreciation of its complex organization.

To characterize the organization of three-dimensional histograms as in Fig. 2, a multifractal analysis [29–31] is realized as follows. The colorimetric cube $[0, Q-1]^3$ is covered by cubic boxes with sidelength a. Each of these boxes, indexed by i, is assigned a measure $P_i \in [0,1]$ equal to the number of pixels of the histogram contained in the box divided by N_{tot}. With a parameter $q \in \mathbb{R}$, one defines a partition function

$$Z(q,a) = \sum_i P_i^q, \tag{1}$$

with the summation index i running over the set of (non-empty) boxes of sidelength a required to cover the three-dimensional histogram. For a fixed value of the exponent q, the evaluation of $Z(q,a)$ is repeated for various box sizes a. The exponent q acts as a zoom on the measure P_i at scale a, by differently distributing the influence on $Z(q,a)$ of the various values of the measure. In this manner, $q > 1$ reinforce, in a relative way, the influence on $Z(q,a)$ of large values of P_i, while $q < 1$ reinforce small P_i. As long as $q > 0$, the order relation of P_i is preserved: large P_i contribute more to $Z(q,a)$ than small P_i, yet with varying weighting according to the value of $q > 0$. At $q < 0$, the order relation of P_i is reversed: small P_i contribute more to $Z(q,a)$ than large P_i, with varying weighting according to the value of $q < 0$. As a result, according to the exponent q, the partition function $Z(q,a)$ is differently influenced by the measure P_i, offering in this way multiple viewpoint on this measure.

Remarkable properties across scales are identified when the partition function $Z(q,a)$ displays power law evolution [32,30,33] of the form

$$Z(q,a) \sim a^{\tau(q)}, \tag{2}$$

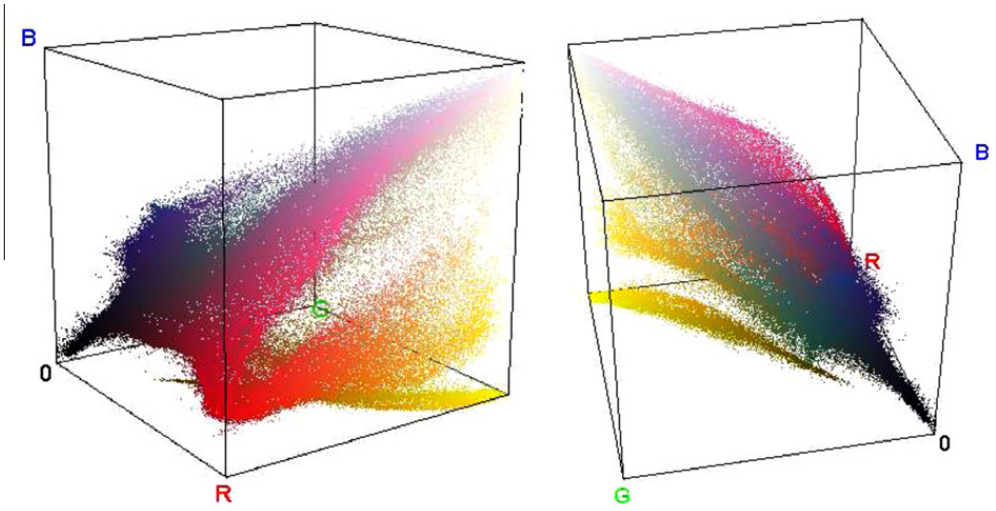

Fig. 2. Three-dimensional histogram in the colorimetric cube $[0, Q-1 = 255]^3$ for image "Flowers" of Fig. 1, under two different angles of view.

with an exponent $\tau(q)$, called mass exponent, a function of the parameter q that provides a condensed characterization of multiscale properties of the structure under analysis. A (trivial) reference behavior is the situation where the pixels of the three-dimensional histogram distribute in a uniform way over the whole colorimetric cube $[0,Q-1]^3$. In this case, the measure of each box is proportional to its volume, i.e. $P_i \sim a^3$, and the number $N(a)$ of boxes with size a required to cover the histogram gives $N(a) \sim a^{-3}$. The partition function of Eq. (1) then yields $Z(q,a) \sim a^{3q-3}$, leading in Eq. (2) to

$$\tau(q) = 3(q-1). \tag{3}$$

A linear mass exponent $\tau(q)$ as in Eq. (3) identifies a monofractal behavior. Power law evolution as in Eq. (2) associated with an exponent $\tau(q)$ departing from a linear form as in Eq. (3), identifies more elaborate multiscale organizations displaying a multifractal character. We note that, as a consequence of normalization to 1 of the measure P_i, one has in Eq. (1) the identity $Z(q=1,a)=1$ for all a; the function $\tau(q)$ of Eq. (2) therefore always verifies $\tau(1)=0$.

A generalized fractal dimension is defined as [27,28]

$$D(q) = \frac{\tau(q)}{q-1}, \tag{4}$$

which reduces to the constant $D=3$ in the case of the uniform three-dimensional histogram of Eq. (3). The generalized fractal dimension $D(q)$ offers another condensed characterization of multiscale properties of the structure under analysis. An interesting special case occurs for $q=0$, when $Z(q=0,a)$ of Eq. (1) reduces to counting the number $N(a)$ of covering boxes at scale a. In this case Eq. (4) gives $D(0)=-\tau(0)$, and through Eq. (2) this number of covering boxes verifies $N(a) \sim a^{-D(0)}$. The dimension $D(0)$ therefore represents the box-counting fractal dimension, or Hausdorff dimension, of the support of the three-dimensional histogram. This dimension is $D(0)=3$ for the support of the uniform three-dimensional histogram; it can be lower than 3 for lacunary histograms with regions void of pixels across a whole range of scales or sizes. Other values of q are associated with special fractal dimensions having simple concrete interpretations [27,28]. In this way $D(q=1)$ is related to the information dimension and $D(q=2)$ to the correlation dimension of the structure under analysis. For the characterization of the three-dimensional histograms from color images, specific studies have been recently performed on the box-counting dimension $D(0)$ of the support in [26], and on the correlation dimension $D(2)$ in [25]. In the present paper, we consider the whole set of generalized fractal dimension $D(q)$ which in principle represents an infinite series of fractal dimensions [27,28], and stands as a more complete characterization of the organization across scales.

3. Multiplicative cascade

As a useful reference, it is possible to distribute the pixels of the three-dimensional color histogram according to a synthesized multifractal measure obtained through the following process [29,34]. The colorimetric cube $[0,Q-1]^3$ is assigned an initial uniform measure of 1. By bisecting equally along each of the three coordinate axes, the colorimetric cube is divided into eight equal sub-cubes. Each of these eight sub-cubes has its initial measure 1/8 multiplied by a weighting factor $m_i \in]0,1[$ with normalization of the weights $\sum_{i=1}^{8} m_i = 1$. This process is iterated, by dividing in eight each of the sub-cubes, and by redistributing the initial measure of each sub-cube according to the weighting by the fixed $\{m_i\}$. The process so iterated implements a multiplicative cascade which converges to a multifractal measure over the colorimetric cube $[0,Q-1]^3$, and whose characteristics are determined by the weighting factors $\{m_i\}$. Especially, with similar notions also addressed in [29,35], the mass exponent $\tau(q)$ of Eq. (2) results as

$$\tau(q) = -\log_2\left(\sum_{i=1}^{8} m_i^q\right), \tag{5}$$

and the generalized fractal dimension $D(q)$ follows from Eq. (4). In particular, one always has for such multiplicative cascade $D(q=0)=3$, in accordance with the support of this multifractal measure which is the whole colorimetric cube, thus a support with dimension 3.

4. Image analysis

We now develop the multifractal analysis based on the partition function $Z(q,a)$ from Eq. (1) numerically evaluated on the histograms associated with three types of color images with size $N_{\text{tot}} = 512 \times 512 = 2^{18}$ pixels and $Q = 256 = 2^8$ levels for each of the three components R, G and B. The first type consists of random images with, at each pixel, the three components R, G and B uniformly drawn at random over $[0,Q-1=255]$. The second type corresponds to images where the pixels distribute over the colorimetric cube $[0,255]^3$ according to the multifractal measure resulting from the multiplicative cascade of Section 3. The third type contains common natural color images, typically as shown in Fig. 1.

On the log–log plots of the partition function $Z(q,a)$ in Figs. 3 and 4, power law behaviors according to Eq. (2) are identified by straight lines. Such straight lines characterizing power laws are clearly visible in Figs. 3 and 4, yet often with a behavior known as crossover, when a change of slope occurs in the power law for a definite scale [36–38]. These observations in Figs. 3 and 4 can be interpreted as follows, keeping in mind that the graphs of $Z(q,a)$ characterize the structure of the color histogram of the image, i.e. the way the pixels of the image take their colors in the colorimetric cube, as a function of scale, from close neighboring colors (small scales) to very distinct colors (large scales).

For the random image of Fig. 3(A), $N_{\text{tot}} = 2^{18}$ pixels take their colors uniformly at random in the colorimetric cube $[0,Q-1]^3$. With $Q = 256 = 2^8$, the colorimetric cube accommodates 2^{24} distinct colors or elementary cells with extent $1 \times 1 \times 1$. The random distribution of $N_{\text{tot}} = 2^{18}$ pixels in these 2^{24} cells yields an average density of $1/2^6$ pixel per cell. In this way, in the neighborhood of a given pixel of the color histogram, below the linear distance of 2^2 there is on average no other pixel. The number of pixels starts

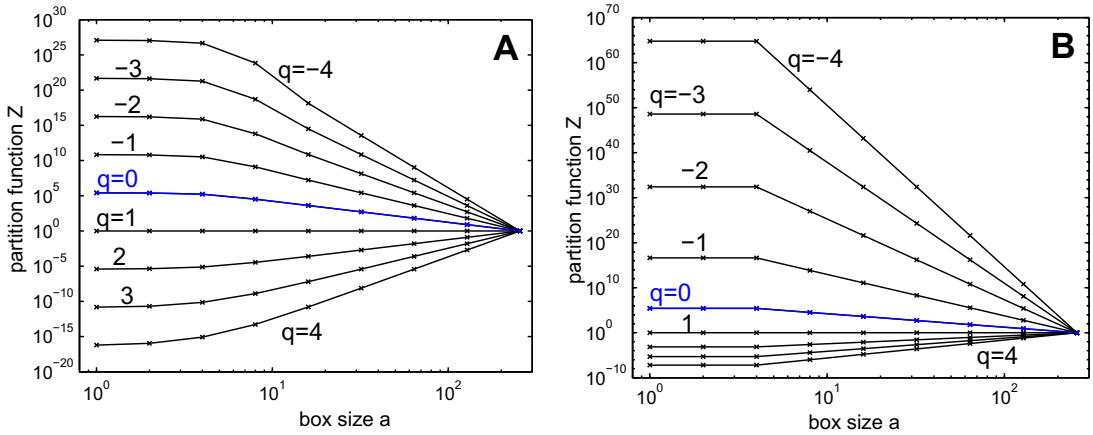

Fig. 3. Partition function $Z(q,a)$ from Eq. (1) as a function of the box size a, for a random uniform image (panel A), and for a multiplicative cascade image with weights $\{m_i\} = \{0.002, 0.039, 0.057, 0.058, 0.094, 0.102, 0.148, 0.500\}$ (panel B).

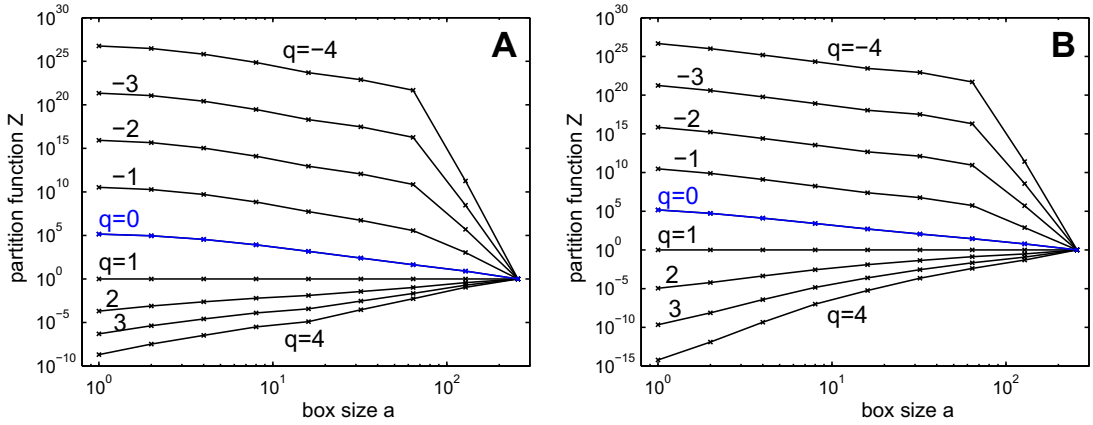

Fig. 4. Partition function $Z(q,a)$ from Eq. (1) as a function of the box size a, for images "Flowers" (panel A) and "Lena" (panel B) of Fig. 1.

to rise, on average, only beyond a neighborhood with linear extension 2^2 and volume $(2^2)^3 = 2^6$. In other words, in the close neighborhood of a color present in the random image, there is no other color employed in the image; one needs to reach to sufficiently distant colors for finding them employed in the image. This is a characteristic of the colorimetric structure of the image. These properties are manifested by the crossover in $Z(q,a)$ around the scale $a = 2^2$ in Fig. 3(A). Scales larger than $a = 2^2$ have to be reached to have the count of pixels start to rise in the histogram; below this scale of $a = 2^2$ the count does not vary and $Z(q,a)$ remains constant. Above the crossover at $a = 2^2$, the variation of $Z(q,a)$ in Fig. 3(A) occurs according to the slope $\tau(q) = 3(q-1)$ of Eq. (3), as shown in Fig. 5(A). This characterizes a uniform distribution of the colors in the three-dimensional histogram above the crossover scale of $a = 2^2$. Accordingly, the generalized fractal dimension $D(q)$ of Eq. (4) is the constant $D = 3$, as shown in Fig. 6(A).

For the image of Fig. 3(B) associated with the multiplicative cascade, a comparable crossover exists at scale $a = 2^2$. The reason is similar. The multiplicative cascade is iterated until it fills 2^{18} sub-cubes of the initial colorimetric cube $[0,255]^3$, matching the $N_{tot} = 2^{18}$ pixels of the considered images. The linear scale $a = 2^2$ is therefore here also a transition scale. Below this crossover scale, the populations of pixels cease to vary, as well as $Z(q,a)$; and above the crossover $a = 2^2$, in Fig. 3(B), $Z(a,q)$ varies according to a power law with slope $\tau(q)$ shown in Fig. 5(A). The corresponding generalized fractal dimension $D(q)$ of Eq. (4) is presented in Fig. 6(A). One observes with the multiplicative cascade for the color histogram, a much different behavior from the uniform histogram of Fig. 3(A). In Fig. 3(B) for the cascade, $Z(q,a)$ above the crossover varies according to a slope $\tau(q)$ much different from that of the uniform histogram. Fig. 5(A) exhibits a nonlinear $\tau(q)$ for the cascade. This is the mark of the multifractal character of the histogram for the cascade of Fig. 3(B). For this histogram, there is no scale where the measure uniformizes. On the contrary, at all scales, the measure keeps on varying in a significant way in the colorimetric space, however with a form of self-similarity across scales of the observed variations. This is manifested by the existence of power laws for $Z(q,a)$, with slopes $\tau(q)$ significantly differing from the slopes attached to the uniform histogram as indicated by Fig. 5(A).

It is to be noted that in Figs. 5 and 6(A), the mass exponents $\tau(q)$ and generalized fractal dimensions $D(q)$ which are numerically evaluated from three-dimensional histograms, exactly match the theoretical predictions from

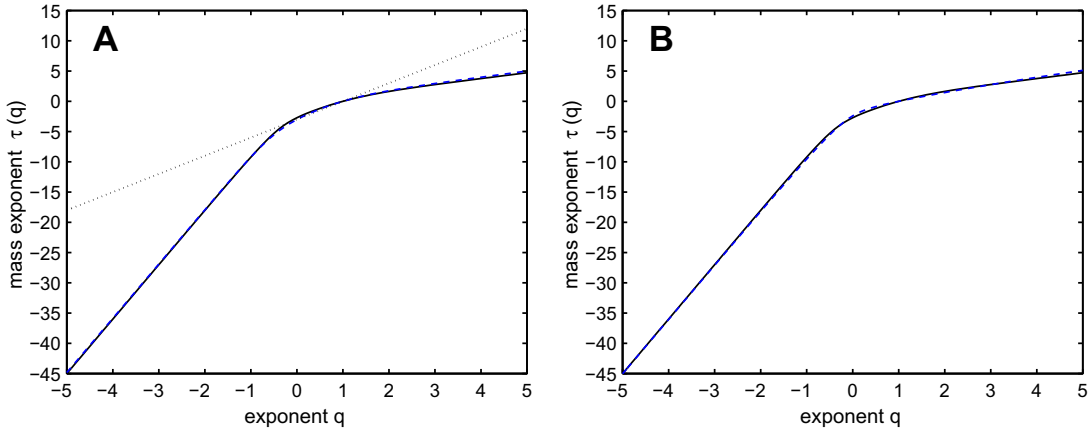

Fig. 5. Mass exponent $\tau(q)$ from Eq. (2) as a function of the exponent q applied to the histogram measure. Panel A: dotted line: uniform image coinciding with the theoretical prediction of Eq. (3); dashed line: multiplicative cascade image of Fig. 3(B) coinciding with the theoretical prediction of Eq. (5); solid line: image "Flowers" of Fig. 1. Panel B: solid line: image "Flowers" of Fig. 1 as in (A); dashed line: image "Lena" of Fig. 1.

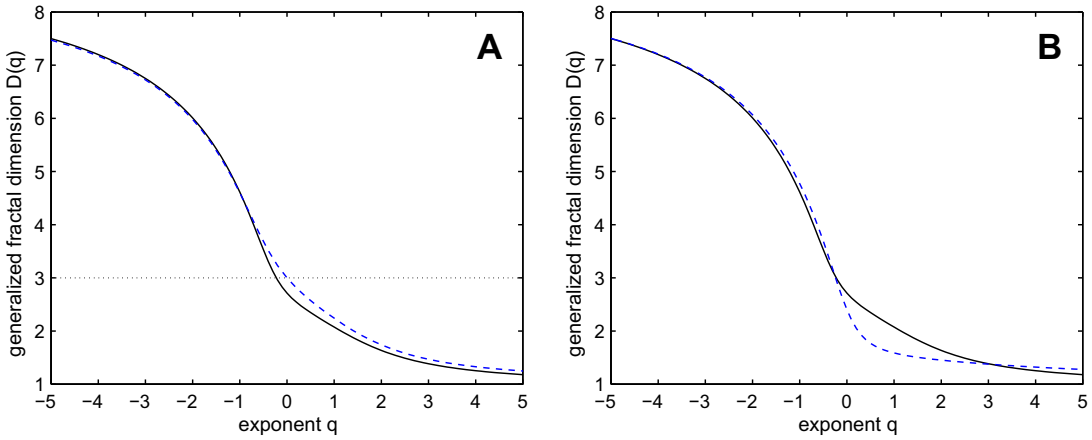

Fig. 6. Generalized fractal dimension $D(q)$ of Eq. (4) as a function of the exponent q applied to the histogram measure. Panel A: dotted line: uniform image coinciding with the theoretical prediction from Eq. (3); dashed line: multiplicative cascade image of Fig. 3(B) coinciding with the theoretical prediction from Eq. (5); solid line: image "Flowers" of Fig. 1. Panel B: solid line: image "Flowers" of Fig. 1 as in (A); dashed line: image "Lena" of Fig. 1.

Eqs. (3)–(5), for the uniform image and for the image associated with the multifractal cascade. This provides a validation, on reference cases, of the procedure for numerical evaluation.

For the natural color images of Fig. 4, an interpretation can be proposed in relation to the previous reference behaviors. Power laws also exist for $Z(q,a)$ in Fig. 4 for the natural images. And for the negative q, a crossover gradually emerges as q moves toward $-\infty$. The crossover is observed this time at a larger scale $a = 2^6$. This crossover identifies a transition in the distribution of the pixels in the color histogram. At large scales $a \geqslant 2^6$, one characterizes colors largely distinct in the image, their relative weights and the way they distribute in the colorimetric space. At small scales $a < 2^6$, one characterizes neighboring colors in the image, that is, fine variations or shades of colors. It can be noted that, contrary to the Fig. 3, below the crossover $a = 2^6$ in Fig. 4 the partition function $Z(q,a)$ keeps on varying. This reveals that in natural images, at short distances from a populated color of the histogram, there generally always exist other colors present in the image, and this down to the finest scales of the colorimetric space. This is a characteristic of natural images, a high richness of color shades manifested by the graphs of $Z(q,a)$. Briefly, on the graphs of Fig. 4, above the crossover one characterizes largely distinct colors, below one characterizes shades of colors. The distributions of these colors exhibit a form of self-similarity across scales, indicated by the power laws, yet with exponents (slopes) differing on both sides of the crossover. It therefore appears that basic colors and shades distribute differently in the colorimetric space, although both in a self-similar manner. Furthermore, it can be verified that if one reduces the RGB color images like those of Fig. 1 into indexed images with a colormap containing only the dominant colors, it then appears that at small scales the graphs of $Z(q,a)$ no longer vary, and become constant as in Fig. 3: the color shades have been lost by keeping only the dominant colors. One has access in this way, through the graphs of $Z(q,a)$ as those of Fig. 4, to a quantitative characterization of the colorimetric organization, that appears rich for natural images.

For the natural color images, Fig. 5(B) shows the slopes $\tau(q)$, with for $q < 0$ the slopes $\tau(q)$ evaluated at large scales above the crossover, for comparison with the conditions of

Fig. 5(A). The corresponding generalized fractal dimension $D(q)$ of Eq. (4) is presented in Fig. 6(B).

The condensed characterizations provided by Figs. 5 and 6 reveal that the behavior of the (non multifractal) uniform image is markedly different from the behavior of the multifractal cascade and from that of the natural images. For the multifractal cascade in Fig. 3(B), the weights $\{m_i\}$ have been chosen to obtain a mass exponent $\tau(q)$ of the cascade that closely matches the mass exponent $\tau(q)$ observed for the natural image "Flowers" in Fig. 5(A). The ensuing generalized dimension $D(q)$ in Fig. 6(A) is also close for the cascade and image "Flowers". This manifests that the multifractal characteristics observed on the natural image "Flowers" are closely similar to those of the reference multifractal behavior supplied by the cascade. For another natural image, "Lena" of Fig. 1, the characteristics observed in Figs. 5 and 6(B) are also of this same kind of multifractal behavior, although some difference exists in the quantitative values of the dimension $D(q)$ in Fig. 6(B) between two distinct natural images. In addition, one observes in Fig. 6(A), at $q = 0$, a dimension $D(q = 0) = 3$ equally for the uniform image and for the multiplicative cascade image. This expresses that the dimension of the support of the color histogram of these two types of images is 3, which is expected from their homogeneous constitution over the whole colorimetric cube, even for the multifractal cascade image. By contrast, the natural image "Flowers" in Fig. 6 exhibits $D(q = 0) = 2.7$; and for image "Lena" one finds $D(q = 0) = 2.4$. This expresses that the dimension of the support of the histogram of the natural images is non-integer, below 3. This is a fractal dimension manifesting a diffuse character of the support of the three-dimensional histogram, with a lacunary structure of voids across a whole range of sizes or scales containing no color employed in the image, as illustrated in Fig. 2. The support of the histogram constitutes the palette of colors existing in the image, independently of the numbers of pixels holding these colors. This support exhibits a fractal character for the natural images, based on the generalized dimension $D(q = 0)$ which is non-integer: natural images tend to show a fractal color palette. The other characteristics, at $q \neq 0$, in turn, are influenced by the populations or numbers of pixels over the histogram.

5. Small and large scales

We complement in Fig. 7 with the mass exponents $\tau(q)$ and generalized fractal dimension $D(q)$ numerically evaluated also from the graphs of $Z(q,a)$ of Fig. 4 but at small scales a. For the exponents $q \geqslant 0$, the values of $\tau(q)$ and $D(q)$ do not significantly differ when evaluated at small or at large scales. There is a uniform behavior across scales, with a regular power law for $Z(q,a)$ with no crossover. On the contrary, for the exponents $q < 0$, one observes in Fig. 7 the values of $\tau(q)$ and $D(q)$ which depart to become distinct when evaluated at small or large scales. It is still difficult to obtain a completely assured interpretation on the origin of this behavior at $q < 0$ giving rise to the crossover. One reason for this is that at $q < 0$ these are the smallest values of the measure over the histogram that tend to dominate the partition function $Z(q,a)$ of Eq. (1), and thus the influence of measurement noise may here become significant, although the presence and impact of measurement noise are difficult to assess in the common natural color images we are dealing with. It is for such reason that the values more commonly interpretable for multifractal parameters as the generalized dimension $D(q)$, are usually associated with the range $q \geqslant 0$. One has in this way $D(0)$ which provides the fractal dimension of the support of the histogram, $D(1)$ which constitutes its information dimension, and $D(2)$ related to its correlation dimension; and these special and important cases of $D(q)$ are evaluated at quasi identical values at small and large scales as seen in Fig. 7. The parameters $\tau(q)$ and $D(q)$ stemming from the multifractal analysis therefore contain, already at $q \geqslant 0$, rich characterizations of the three-dimensional histogram and further, of the colorimetric organization of the images across scales.

The observations reported here concerning the images of Fig. 1 are typical of the results observed during the multifractal analysis we performed on numerous natural color images (see Table 1). In particular, the behavior of the log–log graphs of $Z(q,a)$ as in Fig. 4, starting with one uniform slope at each $q > 0$ and gradually moving to two distinct slopes at small and large scales separated by a crossover at $q < 0$, is observed in a quasi-systematic way on the many natural color images we tested. The graphs of $Z(q,a)$ in

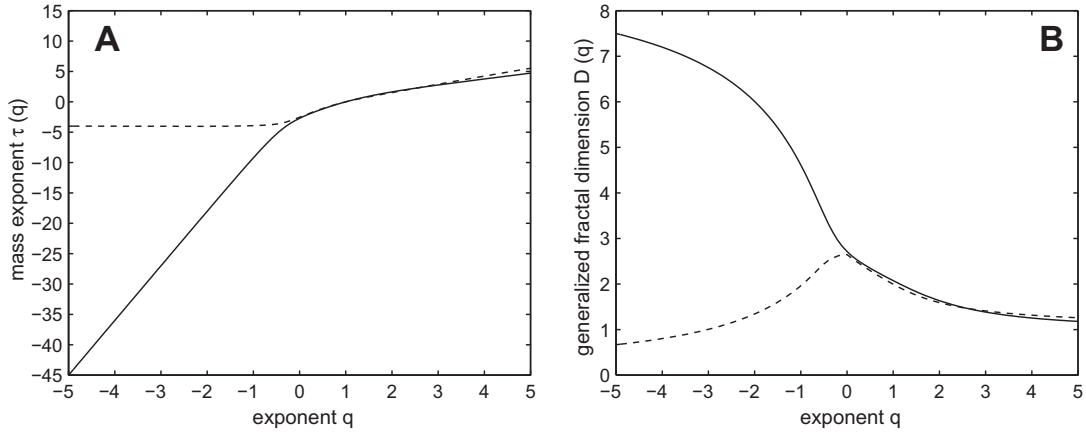

Fig. 7. For the image "Flowers" from Figs. 1 and 4(A), as a function of exponent q. Solid line: at large scales $a \in [2^6, 2^8]$; dashed line: at small scales $a \in [1, 2^6]$. Panel A: mass exponent $\tau(q)$ from Eq. (2). Panel B: generalized fractal dimension $D(q)$ of Eq. (4).

Table 1
For a series of common color images, parameters extracted from their multifractal spectrum $f(\alpha)$ as in Figs. 8 and 12: minimal α_{min} and maximal α_{max} Hölder exponent, spectral width $\Delta\alpha = \alpha_{max} - \alpha_{min}$, exponent $\alpha_0 = \alpha(q = 0)$ achieving the maximum $f(\alpha_0) = D(q = 0)$ of the spectrum providing the box-counting dimension of the support of the color histogram.

Image	α_{min}	α_{max}	$\Delta\alpha$	α_0	$D(0)$
Flowers	0.9	9.0	8.1	3.6	2.7
Lena	1.1	9.0	7.9	4.3	2.4
Sailboat	0.8	9.5	8.7	5.0	2.8
Zelda	1.3	6.4	5.1	2.9	2.3
Boats	0.6	9.1	8.5	4.5	2.4
Monarch	1.1	9.0	7.9	3.6	2.4
Parrots	1.2	8.2	7.0	3.7	2.6
Fruits	1.0	9.5	7.5	4.5	2.5
Yacht	1.3	8.2	6.9	3.9	2.6
Mandrill	1.4	9.1	7.7	4.0	2.8
Goldhill	1.1	8.5	7.4	4.1	2.5
Car	1.3	9.0	7.7	4.1	2.7

Fig. 4 are in this respect typical, together with the forms of the evolutions of $\tau(q)$ and $D(q)$ in Fig. 7. Beyond these similar forms, it is the precise numerical values of $\tau(q)$ and $D(q)$ which are going to differ from one image to the other to become specific. Accordingly for instance for image "Flowers" of Fig. 1 one gets the fractal dimension of the support $D(q = 0) = 2.7$, the information dimension $D(q = 1) = 2.1$, and connected to the correlation dimension $D(q = 2) = 1.6$; while for image "Lena" one finds here $D(q = 0) = 2.4$, $D(q = 1) = 1.8$ and $D(q = 2) = 1.5$.

6. Multifractal spectrum

The multifractal analyses developed above do not require prior hypotheses on the structure of the data to which they are applied. Especially, the partition functions $Z(q,a)$ as in Figs. 3 and 4 can always be computed. One is then in position to judge about the existence of power law behaviors according to Eq. (2), and also about the ranges of scales over which such laws can exist. One already obtains in this way a point of view about properties across scales in the analyzed data. If scaling according to power laws are observed on $Z(q,a)$ over significant ranges of scales, this allows one to extract the slopes $\tau(q)$ in Eq. (2), and then the generalized fractal dimension $D(q)$ via Eq. (4). One gets with $\tau(q)$ and $D(q)$ a condensed characterization of multiscale properties of the three-dimensional (or multidimensional) histogram. By themselves, the multifractal parameters $\tau(q)$ and $D(q)$ provide a useful contribution to the multiscale analysis and characterization of many complex empirical data, as it has been illustrated in many contexts up to the most recent [39,40]. In the context of the present paper, the graphs of $\tau(q)$ and $D(q)$ reflect the colorimetric organization of the images across scales. As such, they can serve various purposes of image processing.

It is possible to push further the multifractal analysis, provided this time to rely on specific hypotheses about the data [29,35,30,31]. One assumes that the local measure P_i at scale a used in Eq. (1) can be expressed as $P_i \sim a^{\alpha}$, where α defines a local singularity exponent or Hölder exponent. One further assumes that the number of boxes of size a where the Hölder exponent takes a definite value α, can be expressed as $N(\alpha,a) \sim a^{-f(\alpha)}$; and in doing so one introduces $f(\alpha)$ which represents the fractal dimension of the set of points with Hölder exponent α, also known as the multifractal spectrum. Based on these assumptions, the mathematical multifractal formalism [29,35,30,31] allows one to establish that, in well defined conditions, the mass exponent $\tau(q)$ that we evaluated, can give access to the multifractal spectrum $f(\alpha)$. This is realized by evaluating the sum of Eq. (1) that defines $Z(q,a)$, no longer as a sum over the boxes i, but as a sum over the values of α present in the data with their respective weights $N(\alpha,a)$. In this way, one can write for the partition function of Eq. (1), a variation with scale a as

$$Z(q,a) \sim \sum_{\alpha} a^{q\alpha - f(\alpha)}. \tag{6}$$

Then, through a saddle point approximation, the sum in Eq. (6) is considered as dominated, at each q, by the value α_q realizing

$$\alpha_q = \arg\min_{\alpha}[q\alpha - f(\alpha)]. \tag{7}$$

One obtains $Z(q,a) \sim a^{q\alpha_q - f(\alpha_q)}$, and by identification with Eq. (2), for each q it comes $\tau(q) = q\alpha_q - f(\alpha_q)$ equivalently obtainable [29,35,30,31] as

$$\tau(q) = \min_{\alpha}[q\alpha - f(\alpha)]. \tag{8}$$

This relation of Eq. (8) indicates that $\tau(q)$ comes as the Legendre transform of $f(\alpha)$, and inversion of this Legendre transform gives [29,35,30,31]

$$f(\alpha) = \min_{q}[q\alpha - \tau(q)]. \tag{9}$$

In this way, through the Legendre transform expressed by Eq. (9), one can deduce the multifractal spectrum $f(\alpha)$ from the mass exponent $\tau(q)$. Also, from Eq. (8), one deduces that $\tau(q = 0)$ corresponds to the minimum of $-f(\alpha)$, or equivalently $-\tau(q = 0)$ corresponds to the maximum of $f(\alpha)$. And as indicated by Eq. (4), one always has $-\tau(q = 0) = D(q = 0)$, so the maximum of the multifractal spectrum $f(\alpha)$ is always $D(0)$, the box-counting dimension the support of the measure.

The relations of Eqs. (8) and (9) provided by the multifractal formalism and connecting the multifractal spectrum $f(\alpha)$ to the mass exponent $\tau(q)$ through a Legendre transform, imply that the functions $f(\alpha)$ and $\tau(q)$ are concave ($\cap$). This is required to have the possibility of deriving $f(\alpha)$ from $\tau(q)$ via Eq. (9). However, the process of evaluating $\tau(q)$ can always be envisaged for a data set, as we performed above, but it will not necessarily always lead to a concave $\tau(q)$, for an empirical data set displaying complex multiscale organization. This seems to be the situation of the three-dimensional histograms from natural color images studied here. For such histograms, the concavity of $\tau(q)$, as illustrated in Fig. 7(A), is usually obtained only over a certain range of scales. This suggests that these three-dimensional color histograms present a more complex multiscale organization, lying beyond the elementary assumptions where the multifractal formalism provides direct access to the spectrum $f(\alpha)$ from the exponent $\tau(q)$. If

we restrict the analysis to the range of scales, as in Fig. 5, where a concave (∩) form can be assigned to $\tau(q)$, it is nevertheless possible in this way to derive, through the Legendre transform of Eq. (9), a multifractal (Legendre) spectrum $f(\alpha)$ attached to the three-dimensional color histogram. This will serve as a further multiscale characterization to situate the three-dimensional histograms in relation to a classic multifractal reference indicator provided by the spectrum $f(\alpha)$.

In this direction, from Eqs. (7) and (8) one can write [41]

$$\tau(q) = q\alpha_q - f(\alpha_q), \tag{10}$$

and since $\tau(q)$ is in a minimum at α_q,

$$0 = \frac{d\tau}{d\alpha_q} = q - \frac{d}{d\alpha_q} f(\alpha_q), \tag{11}$$

whence

$$q = \frac{d}{d\alpha_q} f(\alpha_q). \tag{12}$$

Also, from Eq. (10),

$$\frac{d\tau}{dq} = \alpha_q + q\frac{d\alpha_q}{dq} - \frac{df(\alpha_q)}{d\alpha_q}\frac{d\alpha_q}{dq}, \tag{13}$$

giving, thanks to Eq. (12),

$$\frac{d\tau}{dq} = \alpha_q. \tag{14}$$

For each q where $\tau(q)$ is measured, one thus in practice has access via Eqs. (14) and (10), to a point $(\alpha_q, f(\alpha_q))$ defining the multifractal spectrum.

In this respect, the multifractal spectrum $f(\alpha)$ associated with the multiplicative cascade of Section 3 can be theoretically computed, from Eq. (5), with

$$\alpha_q = \frac{d}{dq}\tau(q) = \frac{-1}{\sum_{i=1}^{8} m_i^q} \sum_{i=1}^{8} m_i^q \log_2(m_i), \tag{15}$$

and

$$f(\alpha_q) = q\alpha_q - \tau(q). \tag{16}$$

As a result, the multifractal spectrum $f(\alpha)$ from Eqs. (15) and (16) lives over a range of Hölder exponent $\alpha \in [\alpha_{\min}, \alpha_{\max}]$, with $\alpha_{\min} = \alpha_{q\to\infty} = -\log_2[\max_i(m_i)]$ and $\alpha_{\max} = \alpha_{q\to-\infty} = -\log_2[\min_i(m_i)]$. In addition, at $q = 0$, the maximum $-\tau(0) = D(0) = 3$ is reached by $f(\alpha)$, and occurs at, from Eq. (15),

$$\alpha_0 = \frac{-1}{8} \sum_{i=1}^{8} \log_2(m_i). \tag{17}$$

Fig. 8 compares the multifractal spectrum $f(\alpha)$ computed from the mass exponent $\tau(q)$ of Fig. 5 for different types of images. In particular in Fig. 8, the weights $\{m_i\}$ of the multiplicative cascade are selected to obtain a range $[\alpha_{\min}, \alpha_{\max}]$ that matches the range observed for the spectrum from the natural color image "Flowers" of Fig. 1. The multifractal spectra $f(\alpha)$ of Fig. 8 are numerically computed, through the Legendre transform of Eq. (9), implemented via Eqs. (14) and (10) in practice, and applied to the mass exponent $\tau(q)$ measured in Fig. 5. At the same time, a theoretical expression is available for $f(\alpha)$ of the multiplicative cascade via Eqs. (15) and (16), and we have verified that an exact match is obtained between the theory and the numerical evaluation of $f(\alpha)$ for the cascade. This provides a validation, against an analytical theory, of the numerical procedure we implemented for the evaluation of the multifractal spectra.

In Fig. 8, for the uniform image, the spectrum degenerates to the single point $(\alpha = 3, f(\alpha = 3) = 3)$ as expected for a measure uniformly filling the colorimetric cube. By contrast in Fig. 8, the spectra $f(\alpha)$ for the multiplicative cascade and for the natural images, display in common a very broad range of Hölder exponent $\Delta\alpha = \alpha_{\max} - \alpha_{\min} \approx 8$, which is the mark of strong multifractal behavior. Also, as we indicated, the maximum of the spectrum $f(\alpha)$ yields the box-counting dimension $D(0)$ of the support of the measure. This dimension is always $D(0) = 3$ for the multiplicative cascade in accordance with its support being the whole colorimetric cube; and this maximum occurs for the cascade at $\alpha_0 \approx 4.04$ according to Eq. (17), as verified in Fig. 8. By contrast, for the natural images in Fig. 8, the maximum of the spectrum is evaluated as $D(0) = 2.7$ for

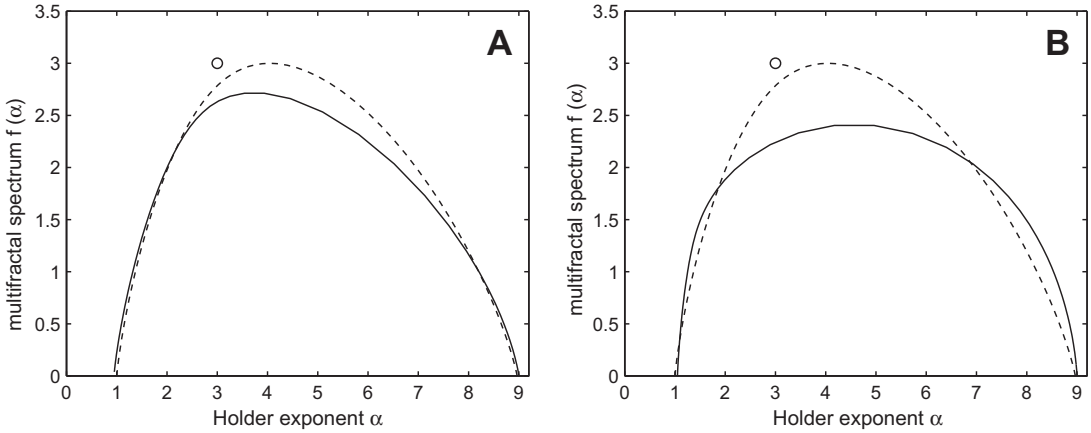

Fig. 8. Multifractal spectrum $f(\alpha)$ as a function of the Hölder exponent α for the histogram measure. Open circle: degenerate spectrum reduced to the point (3,3) for the uniform image. Dashed line: multiplicative cascade image of Fig. 3(B) coinciding with the theoretical prediction of Eqs. (15) and (16). Solid line: image "Flowers" (panel A) and "Lena" (panel B) of Fig. 1.

Fig. 9. Two RGB color images with $N_{tot} = 512 \times 512$ pixels and $Q = 256$ levels.

image "Flowers" of Fig. 8(A) and as $D(0) = 2.4$ for image "Lena" of Fig. 8(B); these are non-integer dimensions below 3 manifesting a nonhomogeneous fractal support of the color histogram in the colorimetric cube. This is an important difference between the multifractal spectra of the cascade and of the natural images: the width $\Delta\alpha$ of these two spectra can always be made to coincide, by proper choice of the weights $\{m_i\}$ of the cascade; but the maximum for the cascade is always at $D(0) = 3$, while it is often observed at a non-integer $D(0) < 3$ with natural images. This represents a more complex multifractal signature from the natural images, with a broad spectrum $f(\alpha)$ and a non-integer fractal dimension $D(0)$ for a nonhomogeneous diffuse structure of the histogram.

For more insight, we also present the same multifractal characterization applied to two other common natural color images from Fig. 9.

For the images in Fig. 9, the partition function $Z(q,a)$ is presented in Fig. 10. With the same approach as for Figs. 5 and 6(B), the corresponding mass exponent $\tau(q)$ and generalized dimension $D(q)$ are shown in Fig. 11. Then Legendre transform of $\tau(q)$ of Fig. 11(A) according to Eq. (9) yields the multifractal spectrum $f(\alpha)$ of Fig. 12.

The nonlinear evolutions of $\tau(q)$ and $D(q)$ observed in Fig. 11, and the broad spectra $f(\alpha)$ in Fig. 12, represent marked multifractal signatures extracted from the three-dimensional color histograms. The dimension $D(0)$ of the support of the histogram, as read for instance at the maximum of the spectrum in Fig. 12, comes as $D(0) = 2.8$ for image "Sailboat" and $D(0) = 2.3$ for image "Zelda". These are non-integer dimensions that identify a fractal support of the histogram. The width of the spectra $\Delta\alpha = \alpha_{max} - \alpha_{min}$ are observed in Fig. 12 as $\Delta\alpha = 8.7$ for image "Sailboat" and $\Delta\alpha = 5.1$ for image "Zelda". The multifractal

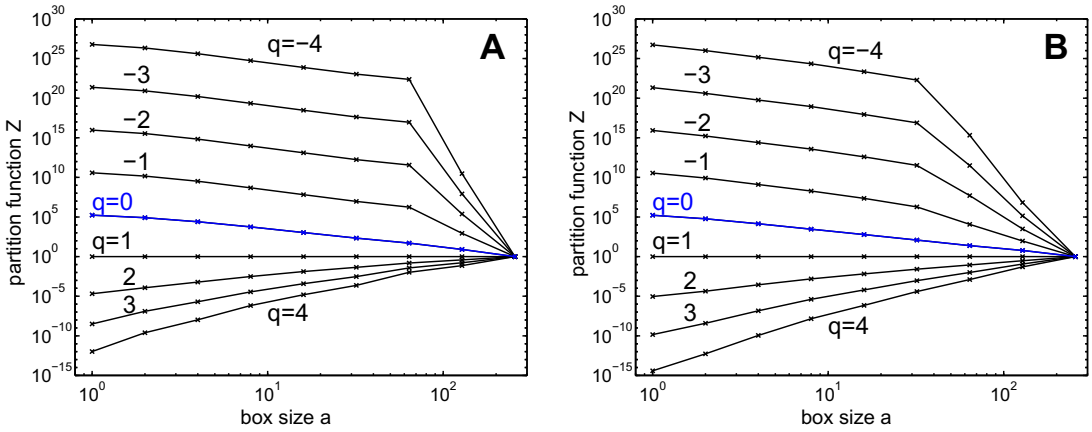

Fig. 10. Partition function $Z(q,a)$ from Eq. (1) as a function of the box size a, for images "Sailboat" (panel A) and "Zelda" (panel B) of Fig. 9.

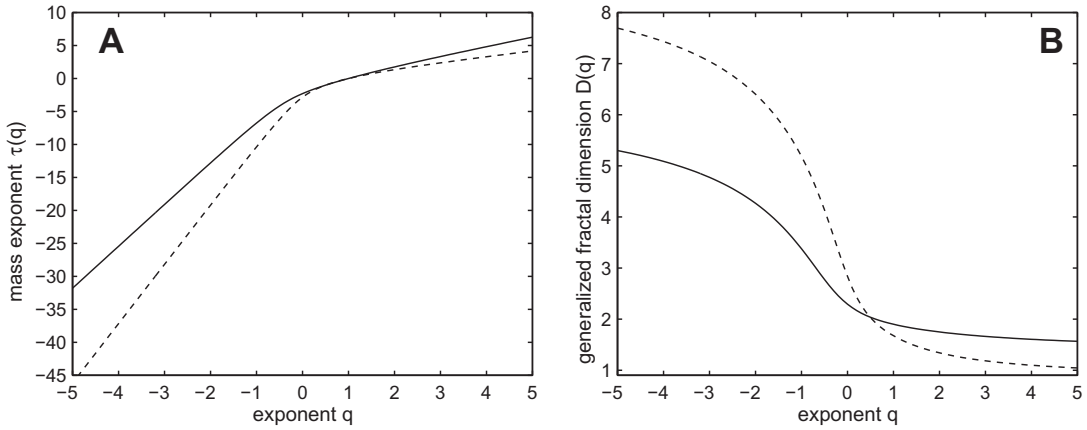

Fig. 11. As a function of the exponent q applied to the histogram measure, mass exponent $\tau(q)$ from Eq. (2) (panel A), and generalized fractal dimension $D(q)$ of Eq. (4) (panel B), for images "Sailboat" (dashed line) and "Zelda" (solid line) of Fig. 9.

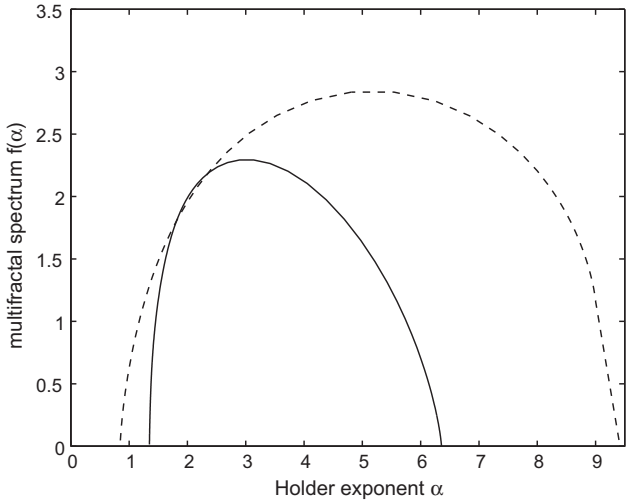

Fig. 12. Multifractal spectrum $f(\alpha)$ as a function of the Hölder exponent α from the histogram of two natural color images. Dashed line: image "Sailboat", solid line: image "Zelda" of Fig. 9.

characteristics measured for different images can thus differ significantly, although the marked multifractal character remains as a common feature.

The same multifractal analyses have been carried out for a whole set of common natural color images, as also used in [26]. Multifractal characteristics measured in this way are summarized in Table 1. These analyses, leading in Table 1 to broad spectral widths $\Delta\alpha$ and non-integer support dimensions $D(0)$, show the general tendency to multifractal behaviors observed from the three-dimensional histograms of natural color images. The quantitative parameters extracted from the present multifractal analysis offer measures to characterize the structures across scales in the color histograms reflecting the colorimetric organizations of images. From previous multifractal analyses applied to the spatial organizations of images, special significance can be attached to specific values of the Hölder exponent α, such as α_0 in Table 1, and they were used to various purposes such as image segmentation or reconstruction [12,6,42,17].

7. Discussion

Multiscale approaches offer means to contribute to the characterization of complex structures such as natural images. In this direction, we have performed a multifractal analysis of the three-dimensional histograms from color images, following an approach which can also be extended to multicomponent images with more than three components. The theoretical framework and equations that we used as a basis for the multifractal analysis are standard material that we reviewed from the literature; and we applied them, for the first time to our knowledge, to a multifractal characterization of the color histograms. The results show complex multiscaling signatures emerging from the analysis of the three-dimensional histograms from natural color images, with behaviors which are similar or even more elaborate than those attached to reference multifractal models provided by three-dimensional multiplicative cascades.

The behaviors observed in the multifractal analysis are useful to image characterization and modeling. They can be related to the presence of multiscale arrangements of the pixels of the color histograms, into clusters with no definite scales. This could carry relevance for methods for segmenting or indexing multicomponent images, that would seek to identify a few well delineated peaks in their histogram, since one can expect organizations with peaks, sub-peaks and sub-sub-peaks, etc., nested across many scales. Also, a colorimetric organization with multifractal character in natural images, could provide cues on coding strategies from the visual system [24] and the distribution of its capabilities across spectral scales, since trichromacy is essentially a coding modality of the visual system. These eventualities were already evoked based on the fractal properties reported in [25,26], and are reinforced by the multifractal properties reported here.

The multifractal characterization of images could also serve other practical applications. For instance, they could be tested to construct metrics for the quantitative assessment of the (colorimetric) perception or realism of natural images as opposed to synthetic images or cartoon-like pictures [43,44]. Multifractal characterization of chromatic structures could also be relevant to novel applications such as artistic painting evaluation and authentication [45,46]. Significant multifractal properties have been reported in different areas of physiology [47–50] and especially in neural dynamics [51–53], inciting one to raise the interesting issue of whether aesthetic relevance could match the brain dynamics.

The multifractal analyses of three-dimensional color histograms are presented here for the first time, as far as we know. They will benefit from extensions to larger series of images, in order to more deeply interpret their meaning and what they reveal concerning the colorimetric organization of natural images. This will consolidate the contribution of fractal and multifractal concepts to the understanding of the complex structures of images.

Acknowledgement

Julien CHAUVEAU acknowledges support from *La Communauté d'Agglomération du Choletais*, France.

References

[1] Jimenez LO, Landgrebe DA. Supervised classification in high-dimensional space: geometrical, statistical, and asymptotical properties of multivariate data. IEEE T Syst Man Cy C 1998;28:39–54.
[2] Landgrebe D. Hyperspectral image data analysis. IEEE Signal Proc Mag 2002;19(1):17–28.
[3] Fisher Y. Fractal Image Compression: Theory and Applications. Berlin: Springer; 1995.
[4] Ruderman DL. Origins of scaling in natural images. Vision Res 1997;37:3385–98.
[5] Turner MJ, Andrews PR, Blackledge JM. Fractal Geometry in Digital Imaging. New York: Academic Press; 1998.
[6] Turiel A, Parga N, Ruderman DL, Cronin TW. Multiscaling and information content of natural color images. Phys Rev E 2000;62:1138–48.
[7] Truong TK, Kung CM, Jeng JH, Hsieh ML. Fast fractal image compression using spatial correlation. Chaos Soliton Fract 2004;22:1071–6.

[8] Wu MS, Teng WC, Jeng JH, Hsieh JG. Spatial correlation genetic algorithm for fractal image compression. Chaos Soliton Fract 2006;28:497–510.
[9] Gousseau Y, Roueff F. Modeling occlusion and scaling in natural images. SIAM J Multiscale Model Simul 2007;6:105–34.
[10] Ruderman DL, Bialek W. Statistics of natural images: scaling in the woods. Phys Rev Lett 1994;73:814–7.
[11] Hsiao WH, Millane RP. Effects of occlusion, edges, and scaling on the power spectra of natural images. J Opt Soc Am A 2005;22:1789–97.
[12] Lévy Véhel J, Mignot P. Multifractal segmentation of images. Fractals 1994;2:371–7.
[13] Sarkar N, Chaudhuri B. Multifractal and generalized dimensions of gray-tone digital images. Signal Process 1995;42:181–90.
[14] Falco T, Francis F, Lovejoy S, Schertzer D, Kerman B, Drinkwater M. Universal multifractal scaling of synthetic aperture radar images of sea-ice. IEEE T Geosci Remote 1996;34:906–14.
[15] Turiel A, Parga N. The multifractal structure of contrast changes in natural images: from sharp edges to textures. Neural Comput 2000;12:763–93.
[16] Du G, Yeo TS. A novel multifractal estimation method and its application to remote image segmentation. IEEE T Geosci Remote 2002;40:980–2.
[17] Turiel A. Relevance of multifractal textures in static images. Electronic Lett Comput Vision Image Anal 2003;1:35–49.
[18] Xia Y, Feng D, Zhao R. Morphology-based multifractal estimation for texture segmentation. IEEE T Image Process 2006;15:614–23.
[19] Chainais P. Infinitely divisible cascades to model the statistics of natural images. IEEE T Pattern Anal 2007;29:2105–19.
[20] Pesquet-Popescu B, Lévy Véhel J. Stochastic fractal models for image processing. IEEE Signal Proc Mag 2002;19(5):48–62.
[21] Srivastava A, Lee AB, Simoncelli EP, Zhu SC. On advances in statistical modeling of natural images. J Math Imaging Vis 2003;18:17–33.
[22] Chen YC, Ji Z, Hua C. Spatial adaptive Bayesian wavelet threshold exploiting scale and space consistency. Multidim Syst Sign P 2008;19:157–70.
[23] Knill DC, Field D, Kersten D. Human discrimination of fractal images. J Opt Soc Am A 1990;7:1113–23.
[24] Olshausen BA, Field DJ. Vision and the coding of natural images. Am Sci 2000;88:238–45.
[25] Chapeau-Blondeau F, Chauveau J, Rousseau D, Richard P. Fractal structure in the color distribution of natural images. Chaos Soliton Fract 2009;42:472–82.
[26] Chauveau J, Rousseau D, Chapeau-Blondeau F. Fractal capacity dimension of three-dimensional histogram from color images. Multidim Syst Sign P 2010;21:197–211.
[27] Hentschel HGE, Procaccia I. The infinite number of generalized dimensions of fractals and strange attractors. Physica D 1983;8:435–44.
[28] Halsey TC, Jensen MH, Kadanoff LP, Procaccia I, Shraiman BI. Fractal measures and their singularities: the characterization of strange sets. Phys Rev A 1986;33:1141–51.
[29] Evertsz CJG, Mandelbrot BB. Multifractal measures. In: Peitgen HO, Jürgens H, Saupe D, editors. Chaos and Fractals – New Frontiers of Science. Berlin: Springer; 1992. p. 921–53.
[30] Harte D. Multifractals: Theory and Applications. London: Chapman and Hall; 2001.
[31] Abry P, Gonçalvès P, Lévy Véhel J. Scaling, Fractals and Wavelets. New York: Wiley; 2009.
[32] Schroeder M. Fractals, Chaos, Power Laws. New York: Freeman; 1991.
[33] Havlin S, Buldyrev SV, Goldberger AL, Mantegna RN, Ossadnik SM, Peng CK, et al. Fractals in biology and medicine. Chaos Soliton Fract 1995;6:171–201.
[34] Stanley HE, Meakin P. Multifractal phenomena in physics and chemistry. Nature 1988;335:405–9.
[35] Beck C, Schlögl F. Thermodynamics of Chaotic Systems. New York: Cambridge University Press; 1993.
[36] Adrover A, Schwalm W, Giona M, Bachand D. Scaling and scaling crossover for transport on anisotropic fractal structures. Phys Rev E 1997;55:7304–12.
[37] Liljenstam M, Ogielski AT. Crossover scaling effects in aggregated TCP traffic with congestion losses. ACM SIGCOMM Comput Commun Rev 2002;32:89–100.
[38] Muñoz-Diosdado A, Guzmán-Vargas L, Ramírez-Rojas A, Del Río-Correa JL, Angulo-Brown F. Some cases of crossover behavior in heart interbeat and electroseismic time series. Fractals 2005;13:253–63.
[39] Ivanov PC, Ma QD, Bartsch RP, Hausdorff JM, Nunes Amaral LA, Schulte-Frohlinde V, et al. Levels of complexity in scale-invariant neural signals. Phys Rev E 2009;79:041920,1–1.
[40] Buard B, Mahé G, Chapeau-Blondeau F, Rousseau D, Abraham P, Humeau A. Generalized fractal dimensions of laser Doppler flowmetry signals recorded from glabrous and non glabrous skin. Med Phys 2010;37:2827–36.
[41] Mallat S. A Wavelet Tour of Signal Processing. Burlington: Academic Press; 1999.
[42] Turiel A, del Pozo A. Reconstructing images from their most singular fractal manifold. IEEE T Image Process 2002;11:345–50.
[43] Mao X, Chen B, Muta I. Affective property of image and fractal dimension. Chaos Soliton Fract 2003;15:905–10.
[44] J. Chauveau, D. Rousseau, P. Richard, F. Chapeau-Blondeau, Fractal analysis tools for characterizing the colorimetric organization of digital images: case study using natural and synthetic images, in: Proceedings VISAPP International Conference on Computer Vision Theory and Applications, Vol. 2, Angers, France, 17–21 May 2010, pp. 245–248.
[45] Mureika JR, Dyer CC, Cupchik GC. On multifractal structure in nonrepresentational art. Phys Rev E 2005;72. 046101,1–15.
[46] Taylor RP, Guzman R, Martin TP, Hall GDR, Micolich AP, Jonas D, et al. Authenticating Pollock paintings using fractal geometry. Pattern Recogn Lett 2007;28:695–702.
[47] Stanley HE, Amaral LAN, Goldberger AL, Havlin S, Ivanov PC, Peng CK. Statistical physics and physiology: monofractal and multifractal approaches. Physica A 1999;270:309–24.
[48] Ivanov PC, Amaral LAN, Goldberger AL, Havlin S, Rosenblum MG, Struzik ZR, et al. Multifractality in human heartbeat dynamics. Nature 1999;399:461–5.
[49] Humeau A, Buard B, Chapeau-Blondeau F, Rousseau D, Mahé G, Abraham P. Multifractal analysis of central (electrocardiography) and peripheral (laser Doppler flowmetry) cardiovascular time series from healthy human subjects. Physiological Measurement 2009;30:617–29.
[50] Su ZY, Wu T, Wang SY. Local scaling and multifractal spectrum analyses of DNA sequences - GenBank data analysis. Chaos Soliton Fract 2009;40:1750–65.
[51] Bershadskii A, Dremencov E, Fukayma D, Yadid G. Multifractal properties of brain neuron signals. Europhys Lett 2002;58:306–11.
[52] Zheng Y, Gao J, Sanchez JC, Principe JC, Okun MS. Multiplicative multifractal modeling and discrimination of human neuronal activity. Phys Lett A 2005;344:253–64.
[53] Suckling J, Wink AM, Bernard FA, Barnes A, Bullmore E. Endogenous multifractal brain dynamics are modulated by age, cholinergic blockade and cognitive performance. J Neurosci Meth 2008;174:292–300.